

RePack then Refine: Efficient Diffusion Transformer with Vision Foundation Model

Guanfang Dong¹ Luke Schultz¹ Negar Hassanpour¹ Chao Gao¹

Abstract

Semantic-rich features from Vision Foundation Models (VFMs) have been leveraged to enhance Latent Diffusion Models (LDMs). However, raw VFM features are typically high-dimensional and redundant, increasing the difficulty of learning and reducing training efficiency for Diffusion Transformers (DiTs). In this paper, we propose RePack then Refine, a three-stage framework that brings the semantic-rich VFM features to DiT while further accelerating learning efficiency. Specifically, the RePack module projects the high-dimensional features onto a compact, low-dimensional manifold. This filters out the redundancy while preserving essential structural information. A standard DiT is then trained for generative modeling on this highly compressed latent space. Finally, to restore the high-frequency details lost due to the compression in RePack, we propose a Latent-Guided Refiner, which is trained lastly for enhancing the image details. On ImageNet-1K, RePack-DiT-XL/1 achieves an FID of 1.82 in only 64 training epochs. With the Refiner module, performance further improves to an FID of 1.65, significantly surpassing latest LDMs in terms of convergence efficiency. Our results demonstrate that packing VFM features, followed by targeted refinement, is a highly effective strategy for balancing generative fidelity with training efficiency.

1. Introduction

The landscape of Latent Diffusion Models (LDMs) has evolved significantly since the success of Stable Diffusion (Rombach et al., 2021). While early models relied on Variational Autoencoders (VAEs) (Kingma & Welling, 2013) to compress images into a latent space, recent methods (Yao et al., 2025; Zheng et al., 2025; Shi et al., 2025b) directly leverage powerful Vision Foundation Models (VFMs), such as CLIP (Radford et al., 2021) and DINOv2/v3 (Oquab et al., 2023; Siméoni et al., 2025), as feature encoders.

Algorithms for integrating VFMs generally fall into two

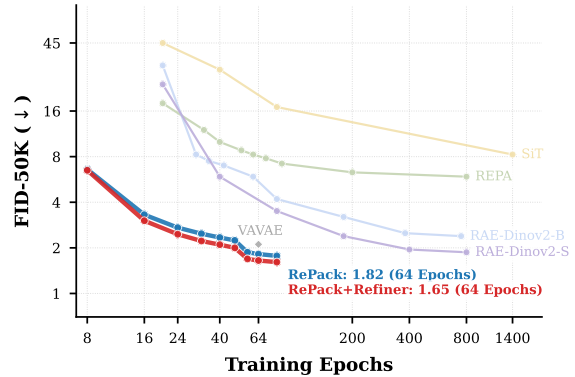


Figure 1: **FID-50K vs. Training Epochs on ImageNet 256 × 256.** RePack achieves strong image generation quality with fewer training epochs. Baseline results are adapted from RAE (Zheng et al., 2025). Notably, RePack exhibits a clear drop in FID at 42 epochs, which is attributed to a scheduled learning rate decay. We find that stage-wise learning rate decay leads to lower FID than using a standard learning rate scheduler.

categories. The first category, represented by VA-VAE (Yao et al., 2025), maintains a standard VAE architecture while using projection heads to align the generative latent space with the VFM feature space during training. Despite benefiting from strong reconstruction capabilities, these methods often use complicated loss functions for balancing the optimization directions, compromising the rich semantic features of the VFMs. This ultimately slows down the learning of the Diffusion Transformer (DiT). The second category, including RAE (Zheng et al., 2025) and SVG (Shi et al., 2025b), adopts frozen VFM features directly as latent representations under the assumption that richer representations should yield superior generation performance. Since most encoder parameters remain frozen, these methods are typically easier to train. Consequently, the practice of feeding these raw, high-density features directly into the Diffusion Transformer (DiT) (Peebles & Xie, 2023) has become a new trend. We provide a comprehensive discussion of related work in Appendix B.

In this paper, we argue that direct use of raw VFM features is suboptimal, as it overlooks the fundamental purpose of the encoder: **information compression**. For ex-

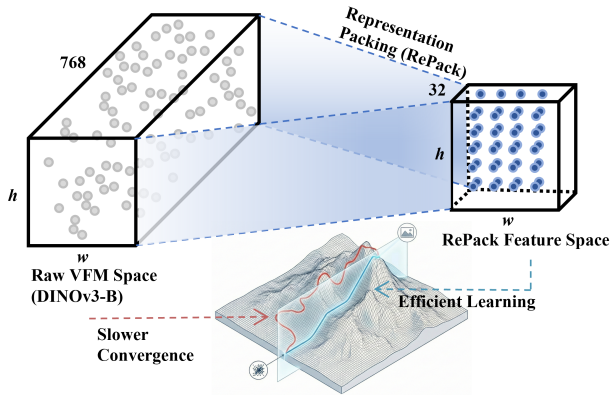


Figure 2: **Design Philosophy of RePack.** We project high-dimensional raw VFM features (768 channels) into a compact RePack feature space (32 channels). The bottom schematic illustrates learning difficulties: a redundant high-dimensional space leads to slower convergence (red path), while a lower-dimensional semantic space provides a smoother optimization path that enables efficient learning (blue path).

ample, when using a standard ViT encoder like DINOv3-B/16, the extracted feature map typically has dimensions of $(768, H/16, W/16)$. We observe that the total number of numerical elements in these features is identical to the original image $(768/16^2 = 3)$, matching the three RGB channels). However, since semantic information intrinsically lies on a low-dimensional manifold (Bengio et al., 2013), performing diffusion in such a high-dimensional space is both inefficient and computationally demanding. The model has to learn a distribution dominated by redundant information that is less important for semantic structure. As illustrated in Figure 2 (Left), this significantly increases the complexity of distribution modeling. This can also be extrapolated by comparing the empirical convergences of RAE and VA-VAE. Despite the fact that RAE is designed to be semantically richer, in reality, it learns slower than the VFM-supervised VA-VAE, which operates on a compressed 32-channel space (VA-VAE at 64 epochs: 2.11 FID; RAE at 80 epochs: 4.28 FID), as shown in Figure 1.

Motivated by the need to address this issue, we propose **RePack** (Representation Packing) that brings back representation compression to LDMs. As illustrated in Figure 2 (Middle, Right), RePack is designed as a lightweight, bias-free linear projection layer that packs *high-dimensional VFM features* (DINOv3-B, 768-dimensional) into a compact low-dimensional manifold. With a small number of parameters (0.04M), RePack encourages the encoder to focus on the most principal semantic components of the pre-trained VFM. This results in a dense semantic representation, leading to easier generative modeling. In our experiments, RePack-DiT-XL/1 achieves an FID of **1.82** after only 64 training

epochs, significantly outperforming existing methods at the same stage.

To further enhance the image generation fidelity of RePack, we introduce a **Latent-Guided Refiner**. Instead of forcing the RePack encoder to learn textures, which would compromise its semantic efficiency, we offload this task to the Refiner. Specifically, we design the Refiner by referring to the latest advances in Pixel Diffusion Models (PDM) (Ma et al., 2025; Yu et al., 2025b), which explicitly model high-frequency details through specialized pixel-space decoders. Our Refiner leverages the generated latent semantics as guidance to synthesize realistic high-frequency textures that are discarded during the packing process. Consequently, our *RePack then Refine* framework harnesses the complementary strengths of latent and pixel spaces. We design a three-stage training strategy to optimize RePack, DiT, and Refiner modules separately. After RePack successfully learns how to pack VFM features into a compact representation, DiT exhibits faster learning due to the structural coherence in the compact manifold. In the final stage, Refiner is trained for high-fidelity textural reconstruction. In our experiments, with *RePack then Refine*, the FID of RePack-DiT-XL/1 is further improved from 1.82 to **1.65** at 64 DiT training epochs. To our knowledge, this represents the fastest-converging result among all recent methods.

Our contributions are highlighted as follows: 1) We propose **RePack**, a semantic compression framework. By identifying redundancy in raw VFM features, RePack employs a compact manifold bottleneck to filter out noise while preserving core semantics. 2) We demonstrate the efficiency of generative modeling in this compact space. RePack-DiT-XL/1 achieves a state-of-the-art FID of **1.82** in just 64 training epochs. 3) We introduce a **Latent-Guided Refiner** to compensate for the detail loss caused by the lightweight encoder of RePack. By decoupling structure generation from texture refinement, it further improves the performance to an FID of **1.65**.

2. Motivation

2.1. VFM Feature as Latent for Diffusion

Latent Diffusion Models (LDMs) typically decouple the generative process into two stages: perceptual compression and generative modeling. Consider an image $x \in \mathbb{R}^{3 \times H \times W}$, in standard LDMs (Rombach et al., 2021), a VAE encoder compresses x into a low-dimensional latent variable $z \in \mathbb{R}^{c \times h \times w}$, where the channel dimension c typically ranges from 4 to 128. Recent trends propose replacing the trainable VAE encoder with a frozen Vision Foundation Model (VFM). Let \mathcal{E}_ϕ denote a frozen VFM encoder. The extracted feature z_{raw} is given by

$$z_{\text{raw}} = \mathcal{E}_\phi(x) \in \mathbb{R}^{D \times h \times w}, \quad (1)$$

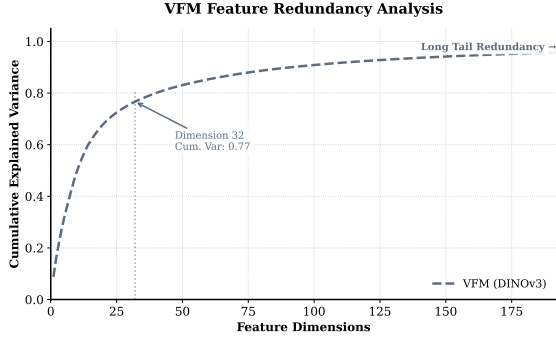


Figure 3: **Analysis of Representation Redundancy.** We perform PCA on features extracted by DINOv3. The cumulative explained variance curve reveals a significant long-tail distribution. Notably, a distinct *Elbow Point* appears around dimension 32, where the curve begins to flatten.

where $(h, w) = (H/p, W/p)$, p is the patch size, and D is the embedding dimension. For a standard ViT-B/16 model, $D = 768$ and $p = 16$. By calculating the total number of elements in z_{raw} , we observe an exact equivalence:

$$h \times w \times D = \frac{H}{16} \times \frac{W}{16} \times 768 = H \times W \times 3. \quad (2)$$

Clearly, the total number of elements in the VFM feature is exactly equal to the number of pixels in the original image. Notably, for larger backbones (e.g., ViT-L with $D = 1024$), the feature space even expands beyond the pixel space. This implies that, in comparison to VAEs, using a VFM as the encoder produces an uncompressed representation. Recent studies have shown that VFMs possess strong semantic extraction capabilities, which can aid DiT learning. However, generative modeling upon an *uncompressed* representation (w.r.t. the number of image pixels) clearly contradicts the core assumption that LDMs should be built upon a compact representation.

2.2. Redundancy Analysis via PCA

To validate our hypothesis that raw VFM features contain high redundancy due to their high dimensionality, we perform a spectral analysis via Principal Component Analysis (PCA). Specifically, we conduct PCA on raw VFM features extracted from the ImageNet-1K validation set using a frozen encoder \mathcal{E}_ϕ (i.e., DINOv3-B). We first extract raw features $z_{\text{raw}} \in \mathbb{R}^{D \times h \times w}$. We then flatten the spatial dimensions to form a feature matrix $\mathbf{Z}_{\text{raw}} \in \mathbb{R}^{M \times D}$, where $M = h \times w$. Singular Value Decomposition (SVD) is performed on the centered covariance matrix of \mathbf{Z}_{raw} . As shown in Figure 3 (grey curve), the cumulative explained variance exhibits a clear long-tail behavior. Notably, we observe a distinct elbow in the curve around dimension 32. The first ~ 32 principal components account for a substantial ma-

jority (approximately 77%) of the total variance. Beyond this point, the curve flattens significantly, indicating that the remaining 700+ dimensions contribute marginally to the variance. Additional analysis is provided in Appendix D.3.

This spectral distribution indicates that the effective semantic information in raw VFM features is concentrated in a low-dimensional manifold, while the high-dimensional remainder is dominated by redundancy. This empirical finding suggests that projecting these features onto a compact subspace may effectively filter out redundancy while preserving core structures.

3. RePack then Refine framework

In light of the observation from the redundancy analysis, we propose a *RePack then Refine* framework for more efficient diffusion learning.

3.1. Architecture Framework

As illustrated in Figure 4, the *RePack then Refine* framework consists of three independent modules: *Representation Packing*, *Generative Modeling*, and *Latent-Guided Refinement*.

Module for Representation Packing. RePack compresses high-dimensional VFM features into a compact manifold through an end-to-end feature mapping and reconstruction pipeline:

$$I_{\text{rec}} = \mathcal{D}_\psi(\mathcal{P}_\theta(\mathcal{E}_\phi(x))), \quad (3)$$

where \mathcal{E}_ϕ is a frozen VFM (e.g., DINOv3-B/16), \mathcal{P}_θ denotes a learnable linear projection, and \mathcal{D}_ψ is the RePack decoder. Given an input image x , raw features $z_{\text{raw}} \in \mathbb{R}^{D \times h \times w}$ are first extracted by the frozen VFM and then mapped by a lightweight projection layer:

$$z = \mathcal{P}_\theta(z_{\text{raw}}), \quad z \in \mathbb{R}^{d \times h \times w}, \quad (4)$$

where $d \ll D$ (e.g., $d = 32$). The projection layer is bias-free, which empirically favors learning a pure subspace projection and leads to improved generation quality.

Module for Generative Modeling. For the generative backbone, we employ LightningDiT (Yao et al., 2025). It is an optimized variant of the standard DiT, which improves convergence efficiency by integrating RMSNorm, SwiGLU, rotary positional embeddings (RoPE), and Rectified Flow. It has been widely adopted as a backbone in related frameworks such as VA-VAE and RAE.

Module for Latent-Guided Refinement. The Refiner adopts a U-Net architecture with skip connections for multi-scale detail propagation. Given a latent feature $z \in \mathbb{R}^{32 \times h \times w}$ and its decoded image $I_{\text{rec}} \in \mathbb{R}^{3 \times H \times W}$, we bilinearly upsample z to $z_{\text{up}} \in \mathbb{R}^{32 \times H \times W}$ and concatenate it with I_{rec} along the channel dimension. The resulting input

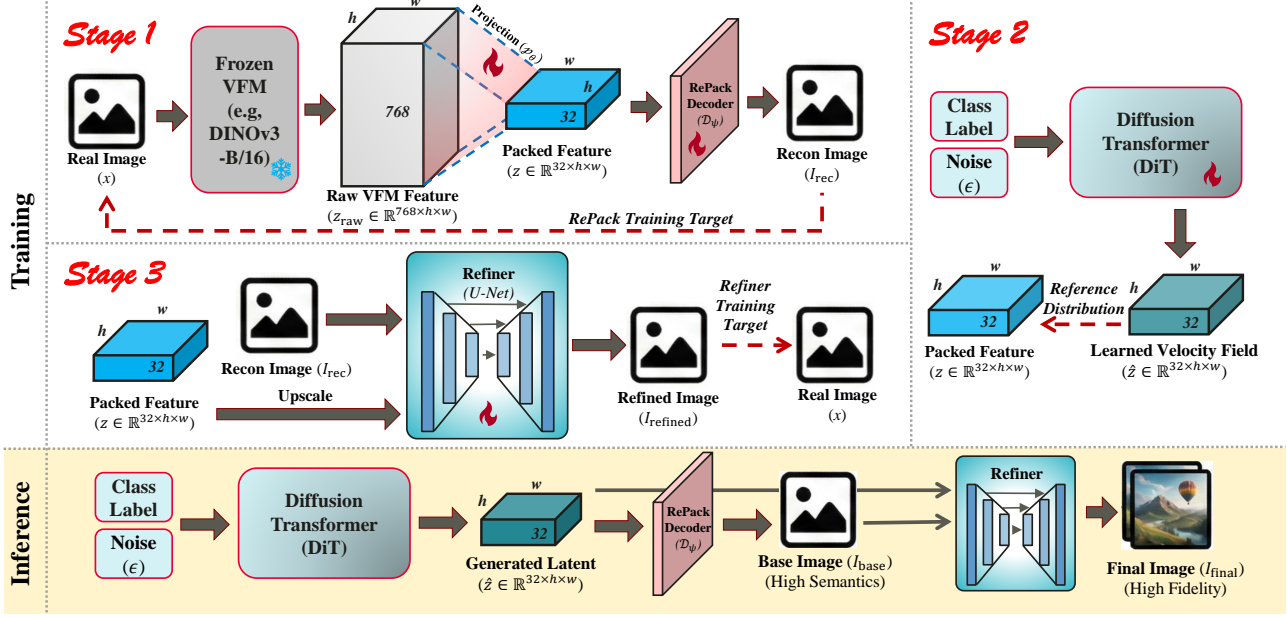


Figure 4: **The RePack then Refine Framework.** The pipeline consists of three stages: (1) **Representation Packing:** Raw VFM features are projected into a compact semantic manifold and reconstructed by the RePack Decoder. (2) **Generative Modeling:** A DiT learns the velocity field over the packed latents. (3) **Latent-Guided Refinement:** A U-Net Refiner restores details using the reconstructed image and upscaled latents. The bottom panel shows the inference flow.

$X_{\text{in}} \in \mathbb{R}^{35 \times H \times W}$ is processed by the Refiner to produce the final output:

$$I_{\text{refined}} = \mathcal{R}(\text{Concat}(I_{\text{rec}}, z_{\text{up}})). \quad (5)$$

3.2. Multi-Stage Training

We optimize the framework in three independent stages.

Stage 1: Representation Packing

In the first stage, we train the projector \mathcal{P}_θ and decoder \mathcal{D}_ψ end-to-end while keeping the VFM \mathcal{E}_ϕ frozen. The objective is to maximize the reconstruction quality of I_{rec} while maintaining a smooth latent manifold. We employ a composite loss $\mathcal{L}_{\text{RePack}}$:

$$\mathcal{L}_{\text{RePack}} = \mathcal{L}_1 + \lambda_{\text{lips}} \mathcal{L}_{\text{lips}} + \lambda_{\text{adv}} \mathcal{L}_{\text{adv}} + \lambda_W \mathcal{L}_{\text{Watson}} + \lambda_f \mathcal{L}_{\text{focal}}. \quad (6)$$

Here, \mathcal{L}_1 is the standard pixel-level reconstruction loss. $\mathcal{L}_{\text{lips}}$ denotes the LPIPS perceptual loss. \mathcal{L}_{adv} represents the adversarial loss from a discriminator to improve perceptual realism. Additionally, $\mathcal{L}_{\text{Watson}}$ (Czolbe et al., 2020) and $\mathcal{L}_{\text{focal}}$ (Jiang et al., 2021) are introduced to enhance visual sensitivity and spectral consistency, respectively.

Stage 2: Generative Modeling

In the second stage, we freeze the RePack encoder and decoder and train the LightningDiT backbone. The generative process is formulated as a flow-matching objective, where

the model learns to predict the velocity field that transforms a standard Gaussian distribution into the data distribution. The training loss minimizes the mean squared error between the predicted and target velocities:

$$\mathcal{L}_{\text{diff}} = \mathbb{E}_{z, \epsilon, t, c} \left[\|\mathbf{v}_t - \mathbf{v}_\phi(z_t, t, c)\|_2^2 \right]. \quad (7)$$

Here, z denotes the clean packed latent features, $\epsilon \sim \mathcal{N}(0, \mathbf{I})$ is Gaussian noise, and $t \in [0, 1]$ is sampled from a logit-normal distribution. The noisy latent is defined as $z_t = tz + (1-t)\epsilon$, with target velocity $\mathbf{v}_t = z - \epsilon$. \mathbf{v}_ϕ denotes the Diffusion Transformer parameterized by ϕ , which predicts the velocity given (z_t, t, c) .

Stage 3: Latent-Guided Refinement

In the final stage, we train the Refiner \mathcal{R} in an **offline** manner, decoupled from the DiT. We construct training pairs using ground-truth images x . First, we extract the latent $z = \mathcal{P}_\theta(\mathcal{E}_\phi(x))$ and reconstruct the base image $I_{\text{rec}} = \mathcal{D}_\psi(z)$. During training, the concatenated input $(I_{\text{rec}}, z_{\text{up}})$ is fed into the Refiner. The model is optimized to recover the high-frequency details of x using a composite objective:

$$\mathcal{L}_{\text{refine}} = \mathcal{L}_1 + \lambda_{\text{lips}} \mathcal{L}_{\text{lips}} + \lambda_{\text{adv}} \mathcal{L}_{\text{adv}}. \quad (8)$$

Here, \mathcal{L}_{adv} denotes the adversarial loss computed using a PatchGAN (Isola et al., 2017) discriminator, which focuses on improving local texture realism at the patch level. By

Table 1: Class-conditional Image Generation Performance on ImageNet 256×256 .

Method	Training Epochs	Backbone Params (M)	VAE Params (M)					Generation Performance				
			Enc.	Enc. _{tr} [†]	Dec.	Total _{tr} [†]	Total	gFID _↓	sFID _↓	IS _↑	Pre. _↑	Rec. _↑
<i>Pixel Diffusion Models (PDM)</i>												
FractalMAR-H (Li et al., 2025)	600	848	–	–	–	–	–	6.15	–	348.9	0.81	0.46
PixelFlow (Chen et al., 2025c)	320	677	–	–	–	–	–	1.98	5.83	282.1	0.81	0.60
PixNerd (Wang et al., 2025)	320	700	–	–	–	–	–	1.95	4.54	300.0	0.80	0.60
JiT (Li & He, 2025)	600	953	–	–	–	–	–	1.86	–	303.0	–	–
DeCo (Ma et al., 2025)	320	682	–	–	–	–	–	1.90	4.47	303.0	0.80	0.61
	600	682	–	–	–	–	–	1.69	4.59	304.0	0.79	0.63
	80	797	–	–	–	–	–	2.36	5.11	282.3	0.80	0.57
PixelDiT (Yu et al., 2025b)	320	797	–	–	–	–	–	1.61	4.68	292.7	0.78	0.64
<i>AutoRegressive (AR) Models</i>												
LlamaGen (Sun et al., 2024)	300	3100	–	–	–	–	72	2.18	5.97	263.3	0.81	0.58
VAR (Tian et al., 2024)	350	2000	–	–	–	–	–	1.80	–	365.4	0.83	0.57
MagViT-v2 (Yu et al., 2023)	1080	307	–	–	–	–	–	1.78	–	319.4	–	–
MAR (Li et al., 2024b)	800	945	–	–	–	–	–	1.55	–	303.7	0.81	0.62
<i>Latent Diffusion Models (LDM)</i>												
MaskDiT (Zheng et al., 2023)	1600	675	34	34	50	84	84	2.28	5.67	276.6	0.80	0.61
DiT (Peebles & Xie, 2023)	1400	675	34	34	50	84	84	2.27	4.60	278.2	0.83	0.57
	64	675	28	28	41	70	70	2.11	4.16	252.3	0.81	0.58
VA-VAE (Yao et al., 2025)	800	675	28	28	41	70	70	1.35	4.15	295.3	0.79	0.65
SiT (Ma et al., 2024)	1400	675	34	34	50	84	84	2.06	4.50	270.3	0.82	0.59
FasterDiT (Yao et al., 2024)	400	675	34	34	50	84	84	2.03	4.63	264.0	0.81	0.60
	64	675	1138	38	476	514	1614	2.01	4.39	250.3	0.83	0.59
FAE (Gao et al., 2025)	80	675	1138	38	476	514	1614	1.92	4.35	249.6	0.83	0.59
	800	675	1138	38	476	514	1614	1.41	4.34	274.1	0.81	0.63
	64	675	1138	38	476	514	1614	1.87	4.39	241.1	0.82	0.59
FAE w/ Time. Shift (Gao et al., 2025)	80	675	1138	38	476	514	1614	1.70	4.33	243.8	0.82	0.61
	800	675	1138	38	476	514	1614	1.29	4.32	268.0	0.80	0.64
MDT (Gao et al., 2023)	1300	675	34	34	50	84	84	1.79	4.57	283.0	0.81	0.61
MDTv2 (Gao et al., 2023)	1080	675	34	34	50	84	84	1.58	4.52	314.7	0.79	0.65
REPA (Yu et al., 2025a)	800	675	34	34	50	84	84	1.42	4.70	305.7	0.80	0.65
RAE (DiT-XL) (Zheng et al., 2025)	800	676	87	0	415	415	502	1.41	–	309.4	0.80	0.63
RAE (DiTDH-XL) (Zheng et al., 2025)	800	839	87	0	415	415	502	1.13	–	262.6	0.78	0.67
	500	675	40	11	43	54	83	2.10	–	258.7	–	–
SVG-XL* (Shi et al., 2025b)	1400	675	40	11	43	54	83	1.92	–	264.9	–	–
RePack	64	675	85.71	0.04	41.42	41.46	127.13	1.82	4.41	269.6	0.83	0.59
	80							1.77	4.42	273.8	0.82	0.59
RePack + Refiner	64	675	85.71	0.04	41.42	97.04	182.71	1.65	4.35	268.9	0.81	0.59
	80							1.61	4.40	272.6	0.81	0.60

* SVG uses 25-step Euler sampling.

[†] Enc_{tr} and Total_{tr} denote the number of trainable parameters in the encoder and the overall VAE pipeline, respectively.

training on reconstruction pairs, the Refiner learns a robust mapping from coarse semantics to fine details, which generalizes well to DiT-generated latents during inference.

3.3. Inference Pipeline

As shown in the bottom panel of Figure 4, image generation is performed using the three trained modules. We first apply the Diffusion Transformer (DiT). Given a class condition c and Gaussian noise $\epsilon \sim \mathcal{N}(0, \mathbf{I})$, it generates a latent representation $\hat{z} \in \mathbb{R}^{32 \times h \times w}$ by integrating the learned velocity field, capturing the global semantic structure of the target image. The generated latent \hat{z} is then decoded into pixel space by the RePack decoder \mathcal{D}_ψ , producing a base image $I_{\text{base}} = \mathcal{D}_\psi(\hat{z})$. Due to the compact latent representation, I_{base} preserves the overall semantic layout. Finally, the Re-

finer takes I_{base} together with the corresponding latent \hat{z} as input and restores high-frequency details conditioned on this structural guidance. The resulting image I_{final} exhibits improved visual fidelity with more realistic textures.

4. Experimental Results

4.1. Implementation Details

We evaluate our framework on ImageNet-1K (Deng et al., 2009) at 256×256 resolution. We utilize a frozen DINOv3 ViT-B/16 (Siméoni et al., 2025) as the feature extractor, followed by the projector and a standard VA-VAE decoder (Yao et al., 2025). RePack and the Refiner are trained for 20 epochs. For generative modeling, we employ DiT-XL/1 and adopt Classifier-Free Guidance (CFG) during inference



Figure 5: **Qualitative Results on ImageNet 256×256 after 64 Training Epochs.** Samples generated by RePack-DiT-XL/1 equipped with the Latent-Guided Refiner.

by default. Comprehensive details regarding model architecture, loss configurations, and additional experimental settings are provided in Appendix A and C.

4.2. Efficiency and Quality Comparison on Image Generation

Overall Results. Table 1 presents the class-conditional generation performance of RePack on ImageNet 256×256 . Remarkably, RePack achieves the fastest learning among all algorithms. With only 64 epochs of training, RePack-DiT-XL/1 achieves an FID of 1.82. By contrast, conventional LDMs (e.g., DiT-XL (Peebles & Xie, 2023)) require 1,400 epochs to reach an FID of 2.27. This shows that a compact and clean latent space can substantially improve training efficiency. Table 1 also shows that, by adding the Latent-Guided Refiner, results are further enhanced: FID is reduced from 1.82 to 1.65, sFID drops to 4.35 and IS reaches 268.9. This confirms the effectiveness of the Refiner. Figure 5 contains a few sample images from **RePack + Refiner**, visually observing fine-grained details.

4.2.1. COMPARISON WITH OTHER VFM ADAPTATION METHODS

- Unlike FAE (Gao et al., 2025), which relies on a computationally expensive encoder (1138M parameters), or PS-VAE (Zhang et al., 2025a) which unfreezes the VFM, RePack prioritizes efficiency and practical utility. FAE’s large parameter count leads to significant memory and latency overheads. Similarly, fine-tuning the VFM (as in PS-VAE) risks catastrophic forgetting, degenerating a robust foundation model into a dataset-specific encoder. By contrast, RePack uses a lightweight non-destructive projector. This minimalist design avoids the heavy computational burden of complex encoders while preserving the VFM’s universal feature space, enabling the DiT to converge signif-

icantly faster.

4.2.2. COMPARISON WITH RAW FEATURE AND FEATURE ALIGNMENT METHODS

Raw-feature methods such as RAE (Zheng et al., 2025) and SVG (Shi et al., 2025b) converge slowly due to high-dimensional sparse representations. RePack is more efficient, achieving an FID of 1.82 after 64 epochs with 41M learnable parameters, compared to RAE (4.28 at 80 epochs, 415M) and SVG (2.10 at 500 epochs, 54M). VA-VAE (Yao et al., 2025) relies on explicit feature alignment, requiring balanced semantic alignment with pixel reconstruction. It reaches an FID of 2.11 after 64 epochs. RePack instead uses a linear projection that preserves the semantic manifold, yielding a cleaner representation while bypassing the optimization conflicts.

4.2.3. COMPARISON WITH PIXEL DIFFUSION MODELS

As in Table 1, our **RePack + Refine** approach achieves stronger results than all six pixel diffusion models (PDMs) on all metrics. For instance, DeCo (Ma et al., 2025) requires 600 epochs to achieve an FID of 1.69. Combining the efficiency of a compact latent space with latent-targeted refinement, our algorithm achieves an FID of 1.65 in 64 epochs. The slow learning of PDMs is due in large part to their operation upon full image pixel space. Designed by borrowing the core strength of PDMs, our latent-guided Refiner decouples high-frequency detail modeling from semantic generation, improving visual detail while retaining the efficiency of latent diffusion models.

4.3. Latent-Guided Refiner Enhances the Modeling of High-Frequency Details

As discussed in Section 2, RePack prioritizes semantic purity and training efficiency by projecting features onto a com-

Table 2: **Effectiveness of the Latent-Guided Refiner across different DiT backbone scales (gFID ↓),** evaluated after 64 training epochs.

Method	DiT-B/1	DiT-B/2	DiT-L/2	DiT-XL/1	DiT-XL/2
RePack	4.12	12.06	4.93	1.82	3.66
RePack + Refiner	3.99	11.98	4.83	1.65	3.20

pact semantic manifold. While this design significantly accelerates DiT convergence, achieving a gFID of 1.82 within 64 training epochs, the extremely low-dimensional bottleneck ($d = 32$) inevitably acts as a low-pass filter, leading to the loss of high-frequency texture information. This effect is reflected in the reconstruction FID (rFID) of 0.83 for the base RePack model.

The Latent-Guided Refiner is specifically designed to address this trade-off. By leveraging the generated latents as structural guidance and explicitly modeling high-frequency details in the pixel domain, the Refiner effectively restores the missing textures. Enabling the Refiner reduces the rFID from 0.83 to 0.69. Correspondingly, the generative performance (gFID) of RePack-DiT-XL/1 is further improved from 1.82 to **1.65**, demonstrating that the Refiner is helpful for achieving high-fidelity generation. To see this, we present a qualitative comparison in Figure 6. The RePack decoded image preserves the overall semantic layout but exhibits reduced fine-grained texture detail. The refined images enhance texture realism, such as the porous texture of the orange peel, while maintaining structural consistency.

Refiner is robust w.r.t different choices of DiTs. It is a question whether the improvement by Refiner is rigidly coupled with a specific choice of DiT. To examine this, we perform multiple learning experiments with five DiTs with different scales, from DiT-B to DiT-XL. As in Table 2, the Refiner consistently improves performance on all DiT model scales.

Application of Refiner to Other VAEs. It is also a question whether the Refiner can be applied to enhance a wide range of VAEs other than RePack itself. We find that for both VA-VAE and SD-VAE, applying Refiner leads a decrease in rFID but an increase in gFID. We believe that the phenomenon that Refiner is most useful with RePack is related to the properties of its compact semantic manifold. Refer to Appendix D.4.3 for detailed analysis.

4.4. How the Latent Representation of RePack is Superior to Others

It is known that the quality of a VAE latent representation can significantly affect the learning of DiT. It is still unclear what the most desired properties are for an effective latent representation. Prior works suggest properties like reduced high-frequency noise (Skorokhodov et al., 2025) and dis-

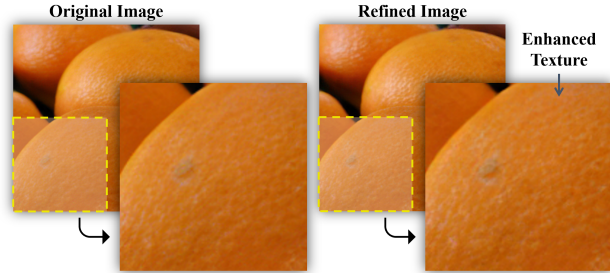


Figure 6: **Effect of Latent-Guided Refinement.** Visual comparison between the base image decoded from RePack latents (Left) and the refined output (Right). As highlighted in the zoomed-in regions, the Refiner recovers realistic high-frequency details, such as the fine porous texture of the orange peel.

entangled structural information from fine-grained details (Chen et al., 2025b). Based on these insights, we hypothesize that an effective latent representation should preserve coherent semantic structure in low-frequency bands while retaining clean, meaningful contours in high-frequency bands. To validate this, we perform a spectral decomposition analysis on the latent codes using a 2D FFT.

As in Figure 7, VA-VAE exhibits strong aliasing artifacts in high-frequency components and blurred structures in low frequencies. By contrast, RePack suppresses aliasing noise while preserving distinct object contours in high frequencies and a sharp, coherent semantic layout in low frequencies. PCA visualizations further show that RePack produces cleaner and more structured latent representations than both VA-VAE and a Standard VAE (i.e., trained from scratch without VFM supervision). Overall, these results indicate that RePack provides a cleaner and more disentangled latent signal. This superior representation simplifies the modeling task for DiT. More experimental details and discussions on latent representations can be found in the Appendix D.2.

4.5. Ablation Studies

Impact of VFMs. We evaluate RePack with different VFM backbones, including DINOv2-B (Oquab et al., 2023), DINOv3-B (Siméoni et al., 2025), MAE (He et al., 2021), and SigLIP (Zhai et al., 2023), using a DiT-B/1 model. Experimental results show that RePack generalizes well across these diverse VFM architectures. In our main experiments, we adopt DINOv3-B as the default backbone to align with the latest developments in Vision Foundation Models. However, as shown in Table 3, DINOv2-B actually achieves the lowest gFID. This result shows that the effectiveness of our framework is not tightly coupled with a specific choice of VFMs. In our main results, we choose DINO-V3 because it is the latest and most widely recognized VFM. Practitioners can easily apply our framework to other VFMs.

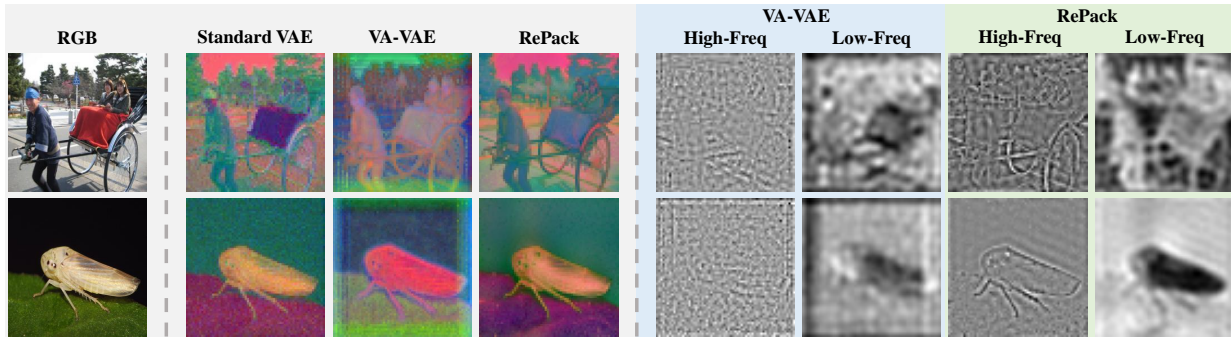


Figure 7: **Visual analysis of latent representations.** **Left:** Input images. **Middle:** PCA visualizations of latents from a Standard VAE (trained w/o VFM guidance), VA-VAE, and RePack. **Right:** Spectral decomposition of VA-VAE and RePack latents.

Table 3: Generation performance (gFID) across different VFM backbones (DiT-B/1, 64 epochs).

Backbone	gFID ↓
MAE (He et al., 2021)	11.66
SigLIP (Zhai et al., 2023)	5.74
DINOv3-B (Siméoni et al., 2025)	4.12
DINOv2-B (Oquab et al., 2023)	3.84

Table 4: Ablation on Projection Layer Design (DiT-B/1, 64 epochs).

Projection Type	PCA	Linear (w/ Bias)	Linear (Bias-free)
gFID ↓	7.56	5.08	4.12

Impact of Projection Layers. We investigate different strategies for implementing the RePack projection layer \mathcal{P}_θ . As shown in Table 4, the learnable bias-free design is the most effective choice. The bias-free projection outperforms the biased variant (gFID 4.12 vs. 5.08) as it performs pure rotation and scaling without introducing unnecessary distribution shifts. For the PCA baseline, we directly project the raw features onto the top-32 principal components calculated from the training set. However, this PCA-based variant performs the worst (gFID 7.56). This suggests that a learnable projection is essential for capturing the semantic manifold structure for DiT training.

Impact of Latent Dimension Sizes. We investigate the impact of the bottleneck dimension d on the trade-off between reconstruction fidelity and generation efficiency. As shown in Table 5, reducing the dimension to $d = 16$ yields the best generative performance (gFID 3.61). This result strongly supports our core hypothesis that a more compact VFM semantic space alleviates the modeling burden for the DiT, leading to faster convergence. However, increasing d to 64 or beyond (Raw 768-dimensional features) provides diminishing returns in reconstruction (rFID) while severely degrading generation quality (gFID increases to

Table 5: Effect of Latent Dimension d on Reconstruction and Generation Performance (DiT-B/1, 64 Epochs).

Dimension (d)	16	32 (Default)	64	768 (Raw)
rFID ↓	1.58	0.83	0.79	0.74
gFID ↓	3.61	4.12	10.18	66.43

66.43). While $d = 16$ offers the fastest convergence, we adopt $d = 32$ as our default setting to align with established baselines. Recent work such as VA-VAE (Yao et al., 2025) and FAE (Gao et al., 2025) all use similar latent channels (e.g., 32). Setting $d = 32$, we strive for a fair comparison w.r.t. baselines, demonstrating that the gains of our framework are not simply a result of reducing d to a lower number.

5. Conclusion

We present *RePack then Refine*, a framework that can harness the semantic richness of VFMs without sacrificing the training efficiency of latent DiTs. The *RePack* module uses a lightweight, bias-free projection to remove redundancy in raw VFM features and compress them into a compact semantic manifold. To compensate for high-frequency detail loss, we propose a *Latent-Guided Refiner* that restores textures in the pixel domain while preserving latent-space structure generation. Experiments show that *RePack then Refine* achieves the fastest learning with high visual fidelity.

Limitations and Future Work Due to computational resource constraints, our largest experiments are obtained with 80 epochs of training. We acknowledge that larger scale experiments may further showcase the strengths of **RePack + Refiner**. Meanwhile, we believe that existing experiments, together with the extensive analysis/visualization in Appendix, are sufficient for supporting our core claims. We leave large experimental studies such as text-to-image generation to future work.

Impact Statement

This paper presents work whose goal is to advance the field of machine learning, particularly in the area of efficient image generation. There are many potential societal consequences of our work, none of which we feel must be specifically highlighted here.

References

- Bengio, Y., Courville, A., and Vincent, P. Representation learning: A review and new perspectives. *IEEE Transactions on Pattern Analysis and Machine Intelligence*, 35(8):1798–1828, 2013. doi: 10.1109/TPAMI.2013.50.
- Bi, T., Zhang, X., Lu, Y., and Zheng, N. Vision foundation models can be good tokenizers for latent diffusion models, 2025. URL <https://arxiv.org/abs/2510.18457>.
- Chen, C., Huang, Z., Zou, C., Zhu, M., Ji, K., Liu, J., Chen, J., Chen, H., and Shen, C. Hieratok: Multi-scale visual tokenizer improves image reconstruction and generation. *arXiv preprint arXiv:2509.23736*, 2025a.
- Chen, J., Zou, D., He, W., Chen, J., Xie, E., Han, S., and Cai, H. Dc-ae 1.5: Accelerating diffusion model convergence with structured latent space. In *Proceedings of the IEEE/CVF International Conference on Computer Vision*, pp. 19628–19637, 2025b.
- Chen, S., Ge, C., Zhang, S., Sun, P., and Luo, P. Pixelflow: Pixel-space generative models with flow. *arXiv preprint arXiv:2504.07963*, 2025c.
- Czolbe, S., Krause, O., Cox, I., and Igel, C. A loss function for generative neural networks based on watson’s perceptual model. *Advances in Neural Information Processing Systems*, 33:2051–2061, 2020.
- Deng, J., Dong, W., Socher, R., Li, L.-J., Li, K., and Fei-Fei, L. Imagenet: A large-scale hierarchical image database. In *2009 IEEE conference on computer vision and pattern recognition*, pp. 248–255. Ieee, 2009.
- Eckart, C. and Young, G. The approximation of one matrix by another of lower rank. *Psychometrika*, 1(3):211–218, 1936. doi: 10.1007/BF02288367.
- Gao, S., Zhou, P., Cheng, M.-M., and Yan, S. Masked diffusion transformer is a strong image synthesizer. In *Proceedings of the IEEE/CVF international conference on computer vision*, pp. 23164–23173, 2023.
- Gao, Y., Chen, C., Chen, T., and Gu, J. One layer is enough: Adapting pretrained visual encoders for image generation. *arXiv preprint arXiv:2512.07829*, 2025.
- He, K., Chen, X., Xie, S., Li, Y., Dollár, P., and Girshick, R. Masked autoencoders are scalable vision learners. *arXiv:2111.06377*, 2021.
- Huang, Z., Zheng, D., Zou, C., Liu, R., Wang, X., Ji, K., Chai, W., Sun, J., Wang, L., Lv, Y., et al. Ming-univision: Joint image understanding and generation with a unified continuous tokenizer. *arXiv preprint arXiv:2510.06590*, 2025.
- Isola, P., Zhu, J.-Y., Zhou, T., and Efros, A. A. Image-to-image translation with conditional adversarial networks. In *Proceedings of the IEEE conference on computer vision and pattern recognition*, pp. 1125–1134, 2017.
- Jiang, D., Wang, M., Li, L., Zhang, L., Wang, H., Wei, W., Dai, G., Zhang, Y., and Wang, J. No other representation component is needed: Diffusion transformers can provide representation guidance by themselves. *arXiv preprint arXiv:2505.02831*, 2025.
- Jiang, L., Dai, B., Wu, W., and Loy, C. C. Focal frequency loss for image reconstruction and synthesis. In *Proceedings of the IEEE/CVF international conference on computer vision*, pp. 13919–13929, 2021.
- Kingma, D. P. and Welling, M. Auto-encoding variational bayes. *arXiv preprint arXiv:1312.6114*, 2013.
- Kouzelis, T., Kakogeorgiou, I., Gidaris, S., and Komodakis, N. Eq-vae: Equivariance regularized latent space for improved generative image modeling, 2025. URL <https://arxiv.org/abs/2502.09509>.
- Leng, X., Singh, J., Hou, Y., Xing, Z., Xie, S., and Zheng, L. Repa-e: Unlocking vae for end-to-end tuning with latent diffusion transformers, 2025. URL <https://arxiv.org/abs/2504.10483>.
- Li, C., Wu, H., Zhang, Z., Hao, H., Zhang, K., Bai, L., Liu, X., Min, X., Lin, W., and Zhai, G. Q-refine: A perceptual quality refiner for ai-generated image. In *2024 IEEE International Conference on Multimedia and Expo (ICME)*, pp. 1–6. IEEE, 2024a.
- Li, T. and He, K. Back to basics: Let denoising generative models denoise. *arXiv preprint arXiv:2511.13720*, 2025.
- Li, T., Tian, Y., Li, H., Deng, M., and He, K. Autoregressive image generation without vector quantization. *Advances in Neural Information Processing Systems*, 37:56424–56445, 2024b.
- Li, T., Sun, Q., Fan, L., and He, K. Fractal generative models. *arXiv preprint arXiv:2502.17437*, 2025.
- Liu, Y., Ouyang, Z., Lou, S., and Song, Y. Omnirefiner: Reinforcement-guided local diffusion refinement. *arXiv preprint arXiv:2511.19990*, 2025.

- Luo, Y., Du, P., Li, B., Du, S., Zhang, T., Chang, Y., Wu, K., Gai, K., and Wang, X. Sample by step, optimize by chunk: Chunk-level grpo for text-to-image generation. *arXiv preprint arXiv:2510.21583*, 2025.
- Ma, N., Goldstein, M., Albergo, M. S., Boffi, N. M., Vanden-Eijnden, E., and Xie, S. Sit: Exploring flow and diffusion-based generative models with scalable interpolant transformers. In *European Conference on Computer Vision*, pp. 23–40. Springer, 2024.
- Ma, Z., Wei, L., Wang, S., Zhang, S., and Tian, Q. Deco: Frequency-decoupled pixel diffusion for end-to-end image generation. *arXiv preprint arXiv:2511.19365*, 2025.
- Medi, T., Wang, H.-Y., Rampini, A., and Keuper, M. Missing fine details in images: Last seen in high frequencies. *arXiv preprint arXiv:2509.05441*, 2025.
- Meng, C., He, Y., Song, Y., Song, J., Wu, J., Zhu, J.-Y., and Ermon, S. Sdedit: Guided image synthesis and editing with stochastic differential equations, 2022. URL <https://arxiv.org/abs/2108.01073>.
- Oquab, M., Darcet, T., Moutakanni, T., Vo, H., Szafraniec, M., Khalidov, V., Fernandez, P., Haziza, D., Massa, F., El-Nouby, A., et al. Dinov2: Learning robust visual features without supervision. *arXiv preprint arXiv:2304.07193*, 2023.
- Page, J., Niu, X., Wu, K., and Gai, K. Boosting latent diffusion models via disentangled representation alignment. *arXiv preprint arXiv:2601.05823*, 2026.
- Peebles, W. and Xie, S. Scalable diffusion models with transformers. In *Proceedings of the IEEE/CVF international conference on computer vision*, pp. 4195–4205, 2023.
- Radford, A., Kim, J. W., Hallacy, C., Ramesh, A., Goh, G., Agarwal, S., Sastry, G., Askell, A., Mishkin, P., Clark, J., et al. Learning transferable visual models from natural language supervision. In *International conference on machine learning*, pp. 8748–8763. PmLR, 2021.
- Rombach, R., Blattmann, A., Lorenz, D., Esser, P., and Ommer, B. High-resolution image synthesis with latent diffusion models. *CoRR*, abs/2112.10752, 2021. URL <https://arxiv.org/abs/2112.10752>.
- Shi, M., Wang, H., Zhang, B., Zheng, W., Zeng, B., Yuan, Z., Wu, X., Zhang, Y., Yang, H., Wang, X., et al. Svg-t2i: Scaling up text-to-image latent diffusion model without variational autoencoder. *arXiv preprint arXiv:2512.11749*, 2025a.
- Shi, M., Wang, H., Zheng, W., Yuan, Z., Wu, X., Wang, X., Wan, P., Zhou, J., and Lu, J. Latent diffusion model without variational autoencoder. *arXiv preprint arXiv:2510.15301*, 2025b.
- Siméoni, O., Vo, H. V., Seitzer, M., Baldassarre, F., Oquab, M., Jose, C., Khalidov, V., Szafraniec, M., Yi, S., Ramamonjisoa, M., et al. Dinov3. *arXiv preprint arXiv:2508.10104*, 2025.
- Skorokhodov, I., Girish, S., Hu, B., Menapace, W., Li, Y., Abdal, R., Tulyakov, S., and Siarohin, A. Improving the diffusability of autoencoders. *arXiv preprint arXiv:2502.14831*, 2025.
- Sun, L., Wu, R., Zhang, Z., Li, R., Sun, Y., Liu, S., and Zhang, L. Beyond external guidance: Unleashing the semantic richness inside diffusion transformers for improved training. *arXiv preprint arXiv:2601.07773*, 2026.
- Sun, P., Jiang, Y., Chen, S., Zhang, S., Peng, B., Luo, P., and Yuan, Z. Autoregressive model beats diffusion: Llama for scalable image generation. *arXiv preprint arXiv:2406.06525*, 2024.
- Team, T. H. Hunyuanimage 2.1: An efficient diffusion model for high-resolution (2k) text-to-image generation. <https://github.com/Tencent-Hunyuan/HunyuanImage-2.1>, 2025.
- Tian, K., Jiang, Y., Yuan, Z., Peng, B., and Wang, L. Visual autoregressive modeling: Scalable image generation via next-scale prediction. *Advances in neural information processing systems*, 37:84839–84865, 2024.
- Tian, Y., Chen, H., Zheng, M., Liang, Y., Xu, C., and Wang, Y. U-repa: Aligning diffusion u-nets to vits. *arXiv preprint arXiv:2503.18414*, 2025.
- Tong, S., Zheng, B., Wang, Z., Tang, B., Ma, N., Brown, E., Yang, J., Fergus, R., LeCun, Y., and Xie, S. Scaling text-to-image diffusion transformers with representation autoencoders. *arXiv preprint arXiv:2601.16208*, 2026.
- Wang, S., Gao, Z., Zhu, C., Huang, W., and Wang, L. Pixnerd: Pixel neural field diffusion. *arXiv preprint arXiv:2507.23268*, 2025.
- Wang, X., Li, Y., Zhang, H., and Shan, Y. Towards real-world blind face restoration with generative facial prior. In *Proceedings of the IEEE/CVF conference on computer vision and pattern recognition*, pp. 9168–9178, 2021.
- Wu, G., Zhang, S., Shi, R., Gao, S., Chen, Z., Wang, L., Chen, Z., Gao, H., Tang, Y., Yang, J., et al. Representation entanglement for generation: Training diffusion transformers is much easier than you think. *arXiv preprint arXiv:2507.01467*, 2025.

- Xu, Y., Luo, S., Wang, L., He, D., and Liu, C. Diagnosing and improving diffusion models by estimating the optimal loss value. *arXiv preprint arXiv:2506.13763*, 2025.
- Yang, J., Li, T., Fan, L., Tian, Y., and Wang, Y. Latent denoising makes good visual tokenizers. *arXiv preprint arXiv:2507.15856*, 2025.
- Yao, J., Wang, C., Liu, W., and Wang, X. Fasterdit: Towards faster diffusion transformers training without architecture modification. *Advances in Neural Information Processing Systems*, 37:56166–56189, 2024.
- Yao, J., Yang, B., and Wang, X. Reconstruction vs. generation: Taming optimization dilemma in latent diffusion models. In *Proceedings of the Computer Vision and Pattern Recognition Conference*, pp. 15703–15712, 2025.
- Yu, L., Lezama, J., Gundavarapu, N. B., Versari, L., Sohn, K., Minnen, D., Cheng, Y., Birodkar, V., Gupta, A., Gu, X., et al. Language model beats diffusion—tokenizer is key to visual generation. *arXiv preprint arXiv:2310.05737*, 2023.
- Yu, S., Kwak, S., Jang, H., Jeong, J., Huang, J., Shin, J., and Xie, S. Representation alignment for generation: Training diffusion transformers is easier than you think. In *The Thirteenth International Conference on Learning Representations*, 2025a. URL <https://openreview.net/forum?id=DJSZGGZYVi>.
- Yu, Y., Xiong, W., Nie, W., Sheng, Y., Liu, S., and Luo, J. Pixeldit: Pixel diffusion transformers for image generation. *arXiv preprint arXiv:2511.20645*, 2025b.
- Zhai, X., Mustafa, B., Kolesnikov, A., and Beyer, L. Sigmoid loss for language image pre-training. In *Proceedings of the IEEE/CVF International Conference on Computer Vision (ICCV)*, pp. 11975–11986, October 2023.
- Zhang, S., Zhang, H., Zhang, Z., Ge, C., Xue, S., Liu, S., Ren, M., Kim, S. Y., Zhou, Y., Liu, Q., et al. Both semantics and reconstruction matter: Making representation encoders ready for text-to-image generation and editing. *arXiv preprint arXiv:2512.17909*, 2025a.
- Zhang, X., Ke, B., Riemenschneider, H., Metzger, N., Obukhov, A., Gross, M., Schindler, K., and Schroers, C. Betterdepth: Plug-and-play diffusion refiner for zero-shot monocular depth estimation. In *The Thirty-eighth Annual Conference on Neural Information Processing Systems*, 2024. URL <https://openreview.net/forum?id=35WwZhkush>.
- Zhang, X., Liao, J., Zhang, S., Meng, F., Wan, X., Yan, J., and Cheng, Y. Videorepa: Learning physics for video generation through relational alignment with foundation models. *arXiv preprint arXiv:2505.23656*, 2025b.
- Zhao, X., Zhang, Z., Huang, Y., Mi, Y., Mu, G., Ding, S., Wang, J., Guo, R., and Zhou, S. Glotok: Global perspective tokenizer for image reconstruction and generation. *arXiv preprint arXiv:2511.14184*, 2025.
- Zheng, B., Ma, N., Tong, S., and Xie, S. Diffusion transformers with representation autoencoders. *arXiv preprint arXiv:2510.11690*, 2025.
- Zheng, H., Nie, W., Vahdat, A., and Anandkumar, A. Fast training of diffusion models with masked transformers. *arXiv preprint arXiv:2306.09305*, 2023.
- Zhou, S., Chan, K., Li, C., and Loy, C. C. Towards robust blind face restoration with codebook lookup transformer. *Advances in Neural Information Processing Systems*, 35: 30599–30611, 2022.
- Zhou, X., Li, Q., Hu, X., Chen, H., and Gu, S. Guiding a diffusion transformer with the internal dynamics of itself. *arXiv preprint arXiv:2512.24176*, 2025.

A. Model Architectures

In this section, we provide detailed architectural specifications for the RePack framework, including the Encoder, Decoder, and the Latent-Guided Refiner.

A.1. RePack Encoder and Decoder

The RePack VAE consists of an asymmetric Encoder-Decoder pair. For the Encoder, we present the configuration that achieved the best performance in our experiments. Specifically, we utilize a frozen **DINOv3-ViT-B/16** backbone followed by a lightweight linear projector. For the Decoder, we adopt the exact architecture used in **VA-VAE** (Yao et al., 2025) to ensure a fair comparison and to demonstrate that our performance gains are due to the packed semantic representation rather than a stronger decoder. The detailed configuration for both components is provided in Table 6.

Table 6: **Detailed Architecture of RePack VAE.** The input resolution is 256×256 . The Encoder compresses images into a $32 \times 16 \times 16$ latent space using a frozen DINOv3 backbone. The Decoder, adopted from VA-VAE (Yao et al., 2025), reconstructs the image from this compact manifold.

Module	Resolution	Channels	Layer Details
<i>Encoder (Frozen Backbone + Projector)</i>			
Input Image	256×256	3	–
ViT Backbone	16×16	768	Frozen DINOv3-B/16 (Patch Features)
Projector	16×16	64	Conv2d 1×1 , bias=False
Latent Sample	16×16	32	Gaussian Sampling (Mean/Std split)
<i>Decoder (Adopted from VA-VAE (Yao et al., 2025))</i>			
Latent Input	16×16	32	Input z
Conv In	16×16	512	Conv2d 3×3
Middle Block	16×16	512	ResBlock \rightarrow Attention \rightarrow ResBlock
Upsample Block 1	32×32	512	ResBlock $\times 3 \rightarrow$ Upsample
Upsample Block 2	64×64	256	ResBlock $\times 3 \rightarrow$ Upsample
Upsample Block 3	128×128	256	ResBlock $\times 3 \rightarrow$ Upsample
Upsample Block 4	256×256	128	ResBlock $\times 3 \rightarrow$ Upsample
Output Block	256×256	128	ResBlock $\times 3 \rightarrow$ Norm \rightarrow Swish
Reconstruction	256×256	3	Conv2d 3×3

Table 7: **Computational Costs and Inference Speed.** Measured on a single V100 GPU with Batch Size = 1 at 256×256 resolution.

Module	Params (M)	GFLOPs	Throughput (img/s)	Peak RAM (MB)
RePack Encoder	85.71	22.35	75.79	504.77
RePack Decoder	41.42	125.82	50.39	622.74
Refiner	55.56	338.18	19.43	582.72

A.2. Latent-Guided Refiner Architecture

The Latent-Guided Refiner is a conditional U-Net designed to restore high-frequency details. It takes the channel-wise concatenation of the base image I_{base} (3 channels) and the bilinearly upsampled latent features z_{up} (32 channels) as input, resulting in 35 input channels. The network follows a U-Net structure with skip connections to propagate fine-grained information from the encoder to the decoder. The detailed configuration for the Refiner is provided in Table 8.

A.3. Computational Complexity and Inference Efficiency

To evaluate the practical deployment costs of RePack, we analyze the computational complexity and memory footprint of each component. Table 7 reports the number of parameters, GFLOPs, inference throughput (img/s), and peak memory usage. All metrics are measured on a single *NVIDIA Tesla V100* GPU with a batch size of 1 to simulate a real inference scenario.

Table 8: **Refiner Architecture (U-Net)**. The model operates at a base channel width of $C = 128$. Skip connections concatenate features from the encoder path to the decoder path. Attention blocks are applied at the 32×32 resolution to capture global context.

Stage	Resolution	Ch (In/Out)	Layer Composition
Input	256×256	$35 \rightarrow 128$	Concat(I_{base}, z_{up}) \rightarrow Conv 3×3
<i>Downsampling Path (Encoder)</i>			
Down 1	$256 \rightarrow 128$	$128 \rightarrow 128$	ResBlock $\times 2 \rightarrow$ Downsample (Stride 2)
Down 2	$128 \rightarrow 64$	$128 \rightarrow 256$	ResBlock $\times 2 \rightarrow$ Downsample (Stride 2)
Down 3	$64 \rightarrow 32$	$256 \rightarrow 512$	ResBlock $\times 2 \rightarrow$ Attention \rightarrow Downsample
<i>Bottleneck</i>			
Middle	32×32	$512 \rightarrow 512$	ResBlock ($512 \rightarrow 1024$) \rightarrow Attn \rightarrow ResBlock ($1024 \rightarrow 512$)
<i>Upsampling Path (Decoder) - Inputs include Skip Connections</i>			
Up 1	$32 \rightarrow 64$	$1024 \rightarrow 512$	Upsample \rightarrow Concat \rightarrow ResBlock \rightarrow Attn
Up 2	$64 \rightarrow 128$	$768 \rightarrow 256$	Upsample \rightarrow Concat \rightarrow ResBlock $\times 2$
Up 3	$128 \rightarrow 256$	$384 \rightarrow 128$	Upsample \rightarrow Concat \rightarrow ResBlock $\times 2$
Output	256×256	$256 \rightarrow 3$	Concat(Skip) \rightarrow ResBlock \rightarrow Norm \rightarrow SiLU \rightarrow Conv \rightarrow Tanh

Analysis of Refiner Complexity. As shown in Table 7, the RePack Encoder and Decoder are efficient, maintaining high throughput with low memory consumption. We observe that the *Refiner* exhibits a higher GFLOPs count (338.18 G) compared to the VAE components. This is expected as the Refiner operates directly on high-resolution pixel inputs (256×256) with 35 channels, whereas the VAE components process data in a compressed latent space. However, it is crucial to note that unlike the Diffusion Transformer (DiT), which requires tens or hundreds of iterative function evaluations during sampling, the Refiner is a single-step feed-forward network. Consequently, despite the higher GFLOPs, it achieves a throughput of 19.43 img/s , which is sufficient for most generation applications. In future work, we plan to further enhance the Refiner’s efficiency by applying model compression techniques, such as pruning and quantization, to reduce computational overhead and further boost throughput.

B. Related Works

B.1. VFM-Driven Latent Representations

Direct High-Dimensional Utilization. Some methods bypass encoder training by using raw VFM features directly as latents. **RAE** (Zheng et al., 2025) and **T2I-RAE** (Tong et al., 2026) utilize frozen features from models like DINOv2, shifting the reconstruction burden to the decoder to maximize semantic richness. Similarly, **SVG** (Shi et al., 2025b) augments frozen DINO features with a lightweight residual branch. This strategy is subsequently scaled to text-to-image synthesis in **SVG-T2I** (Shi et al., 2025a).

Adapted and Compressed VFM Latents. Other approaches project VFM features into lower-dimensional spaces to reduce redundancy. **FAE** (Gao et al., 2025) employs an attention encoder to compress high-dimensional features into compact latents. **VFM-VAE** (Bi et al., 2025) integrates frozen VFMs with a multi-scale fusion decoder to bridge semantic and pixel domains. **Send-VAE** (Page et al., 2026) aligns VAE latents with VFM hierarchies to enhance disentanglement. **PS-VAE** (Zhang et al., 2025a) maps frozen features into a KL-regularized space and jointly optimizes for pixel and semantic consistency to preserve fine-grained textures.

While these methods effectively leverage VFM semantics, direct utilization approaches (e.g., RAE) exhibit slower convergence, and adaptation methods (e.g., FAE, PS-VAE) often involve more complex nonlinear encoders. In contrast, **RePack** explores a lightweight alternative by identifying a low-dimensional structure within VFM features and applying a bias-free linear projection. This design reduces redundancy while avoiding additional architectural complexity.

B.2. Representation Alignment and Distillation

Instead of modifying the latent space architecture, some methods enforce alignment during training via auxiliary losses. **REPA** (Yu et al., 2025a) regularizes diffusion models by aligning noisy states with clean VFM representations. This paradigm is subsequently extended to end-to-end VAE-DiT tuning in **REPA-E** (Leng et al., 2025), U-Net architectures in

U-REPA (Tian et al., 2025), and video generation in **VideoREPA** (Zhang et al., 2025b). **REG** (Wu et al., 2025) takes a different approach by explicitly entangling high-level class tokens with image latents to guide the denoising process. **VA-VAE** (Yao et al., 2025) introduces a VFM alignment loss to regularize the VAE latent space towards semantic distributions without changing the inference architecture.

Alignment strategies improve convergence by introducing auxiliary regularization, while **RePack** follows a different design choice and explicitly constructs the latent space from VFM features via projection. This design avoids additional loss terms and allows the DiT to operate directly on a semantically structured manifold.

B.3. Structural and Spectral Regularization

Some methods accelerate training by optimizing the tokenizer’s internal properties through mathematical or structural constraints, without relying on external VFM guidance. **EQ-VAE** (Kouzelis et al., 2025) encourages equivariance to spatial transformations such as rotation and scaling to smooth the latent manifold. **SE** (Skorokhodov et al., 2025) regularizes spectral properties to enable a coarse-to-fine spectral autoregression. **FA-VAE** (Medi et al., 2025) utilizes wavelet decomposition to explicitly decouple high-frequency details from low-frequency structure. **HieraTok** (Chen et al., 2025a) employs a multi-scale ViT with scale-causal attention to capture hierarchical detail progressively. **DeToK** (Yang et al., 2025) aligns the tokenizer’s latent space with the downstream denoising objective by training the decoder to reconstruct clean images from corrupted latents. These approaches rely on auxiliary constraints to shape the VAE latent space, whereas **RePack** directly leverages the pre-aligned semantic structure of VFMs through projection onto a compact manifold.

B.4. Internal Guidance and Self-Evolution

Recent works also explore accelerating convergence by leveraging the model’s own internal dynamics rather than external teachers. **SRA** (Jiang et al., 2025) aligns weaker early-layer representations with stronger deep-layer ones to provide internal guidance. **IG** (Zhou et al., 2025) utilizes intermediate layer supervision to stabilize gradients and employs self-guidance during sampling to improve quality. **Self-Transcendence** (Sun et al., 2026) aligns shallow features with VAE latents and then applies internal classifier-free guidance to amplify semantic richness. These methods optimize the training trajectory through internal distillation, while **RePack** operates at the level of input representation.

B.5. Unified Frameworks and Optimization Dynamics

Recently, several studies focus on unifying perception and generation or optimizing training dynamics to accelerate convergence. **MingTok** (Huang et al., 2025) unifies image understanding and generation within a continuous autoregressive framework to eliminate quantization errors. **GloTok** (Zhao et al., 2025) captures global semantic relationships via codebook-wise histogram learning. **Xu et al.** (Xu et al., 2025) propose an analytical loss gap metric to diagnose underfitting at specific noise levels, enabling a principled training schedule that prioritizes harder steps. While these works focus on architectural design or loss formulation, **RePack** instead focuses on the efficiency of the latent representation itself.

B.6. Related Methods for the Latent-Guided Refiner

Our Latent-Guided Refiner draws inspiration from Pixel Diffusion Models (PDMs) such as **DeCo** (Ma et al., 2025) and **PixelDiT** (Yu et al., 2025b), which demonstrate the effectiveness of decoupling high-frequency texture modeling from low-frequency semantic generation. Beyond direct generation, refinement techniques are widely adopted to enhance quality or restore details. **SDEdit** (Meng et al., 2022) utilizes a stochastic process that adds noise to a coarse guide and iteratively denoises it to recover realism. **BetterDepth** (Zhang et al., 2024) applies a similar diffusion-based refinement strategy to enhance fine-grained details in zero-shot depth estimation. To improve alignment and fidelity, **OmniRefiner** (Liu et al., 2025) employs Group Relative Policy Optimization to align outputs with high-resolution reference patches, a direction further refined by **Chunk-GRPO** (Luo et al., 2025), which optimizes generation at the temporal chunk level to fix advantage attribution. **Q-Refine** (Li et al., 2024a) introduces a quality-aware pipeline using pixel-level Image Quality Assessment (IQA) maps to strictly guide the restoration of local defects. In specific restoration domains such as blind face restoration, methods often leverage strong external priors. For example, **GFP-GAN** (Wang et al., 2021) utilizes pre-trained GAN priors to recover textures, while **CodeFormer** (Zhou et al., 2022) maps degraded inputs to a discrete codebook to reduce restoration uncertainty. In contrast to these approaches, **RePack** uses the packed latent z as a structural reference. The Refiner operates as a deterministic, offline module and focuses on complementing texture details, while keeping the overall inference pipeline unchanged.

Table 9: Essential training hyperparameters for RePack Stage 1.

Configuration	Value	Loss Weights	Value
Base Learning Rate	1.0×10^{-5}	LPIPS weight (λ_{lips})	0.2
Batch Size	32	Adversarial weight (λ_{adv})	0.5
Embed Dimension	32	FFL weight (λ_f)	0.05
Resolution	256×256	Watson weight (λ_w)	0.005

C. Detailed Configurations

We provide the training hyperparameters for three stages of the RePack framework: the Representation Packing (VAE), the Generative Model (DiT), and the Latent-Guided Refiner.

C.1. Stage 1: Representation Packing (VAE)

The Stage 1 training aims to compress high-dimensional features from a frozen VFM (DINOv3-B/16) into a compact 32-dimensional semantic manifold. By incorporating Focal Frequency Loss (Jiang et al., 2021) and Watson Perceptual’s Loss supervision (Czolbe et al., 2020), the reconstruction quality is enhanced, improving the rFID from 0.8789 to 0.8295. The essential training parameters are summarized in Table 9.

C.1.1. FOCAL FREQUENCY LOSS (FFL)

We employ Focal Frequency Loss (FFL) (Jiang et al., 2021) to adaptively focus on hard-to-reconstruct frequency components. Given the frequency spectra of the real image $F_r(u, v)$ and the reconstructed image $F_f(u, v)$ obtained via 2D DFT, the loss is defined as:

$$\mathcal{L}_{\text{Focal}} = \frac{1}{MN} \sum_{u=0}^{M-1} \sum_{v=0}^{N-1} w(u, v) |F_r(u, v) - F_f(u, v)|^2$$

The spectrum weight matrix $w(u, v)$ is dynamically updated to down-weight easy frequencies and emphasize hard ones:

$$w(u, v) = |F_r(u, v) - F_f(u, v)|^\alpha$$

In our implementation, we set $\alpha = 1.0$ as a balanced trade-off between focus and stability.

C.1.2. WATSON PERCEPTUAL LOSS

Watson Perceptual Loss (Czolbe et al., 2020) aligns the reconstruction with human visual perception. It accounts for luminance masking and contrast masking by normalizing frequency errors with a visibility threshold S_{ijk} :

$$\mathcal{L}_w = \sqrt[p]{\sum_{i,j,k} \left| \frac{C_{ijk} - C'_{ijk}}{S_{ijk}} \right|^p},$$

where C and C' are transform coefficients. This approach prevents the model from being over-penalized by visually imperceptible differences in bright or high-contrast regions, thus preserving more realistic textures in the final reconstruction.

C.2. Stage 2: Generative Modeling (DiT)

For the generative stage, we adopt LightningDiT (Yao et al., 2025), an optimized DiT variant designed for fast convergence and high-fidelity generation. LightningDiT incorporates architectural improvements such as SwiGLU FFN, RMSNorm, and Rotary Positional Embeddings (RoPE).

C.2.1. MODEL AND LOSS CONFIGURATIONS

The model architecture and training loss parameters are detailed in Table 10.

Table 10: LightningDiT-XL/1 Architecture and Loss configurations.

Parameter	Value	Parameter	Value
Architecture		Training / Loss	
Input Channels	32	Path Type	Linear (Rectified Flow)
FFN Type	SwiGLU	Prediction Target	Velocity
Normalization	RMSNorm	Use Logit-Normal	True
Position Embedding	RoPE	Use Cosine Loss	True
		AdamW β_2	0.95

C.2.2. STAGE-WISE TRAINING STRATEGY

We found that a manual stage-wise training strategy, rather than a continuous learning rate scheduler, leads to better convergence and final generative quality. As shown in the Figure 1, we observed a sharp improvement in FID after a manual learning rate adjustment at Epoch 48.

Specifically, we initially train the model with a learning rate of 2.0×10^{-4} . At Epoch 48, the learning rate is dropped to 1.0×10^{-4} . This approach allows the model to first capture global semantic structures and subsequently refine details within the compact manifold. As shown in Table 11, while a standard scheduler achieves a respectable FID of 1.98 at Epoch 64, our manual stage-wise strategy reaches a superior FID of **1.82**.

Table 11: FID-50K performance comparison for DiT-XL/1: LR Scheduler vs. Manual Stage-wise Drop.

Epoch	16	32	48	56	64
Standard Scheduler	3.31	2.53	2.10	1.99	1.98
Manual Stage-wise	3.31	2.48	2.24	1.87	1.82

Scalability of the Stage-wise Strategy. It is worth noting that while the manual learning rate decay yields significant gains for the large-scale DiT-XL/1, this benefit does not generalize to smaller backbones. Experimental results show that applying the same sharp decay strategy to DiT-B/1 results in a gFID of 5.08, which is inferior to the 4.12 achieved with the standard scheduler. Similarly, DiT-B/2 exhibits a slight performance degradation (12.19 vs. 12.06).

C.2.3. NUMERICAL INTEGRATION AND SAMPLING

We attribute this behavior to differences in model capacity and optimization dynamics. Larger models can capture global semantics early and benefit from a sharp learning rate drop for refinement, whereas smaller models require longer exploration with a higher learning rate. As a result, stage-wise decay is effective for large models, while standard scheduling remains more reliable for lightweight backbones.

We evaluate the generative performance of RePack by solving the deterministic Probability Flow Ordinary Differential Equation (ODE) associated with the learned velocity field. Following the Rectified Flow formulation, we utilize a first-order Euler integrator for numerical solution.

To achieve high-fidelity generation and precise class alignment, we employ Classifier-Free Guidance (CFG) with a scale of 15.0. To further optimize the balance between perceptual quality and sample diversity, we incorporate a CFG interval strategy starting at 0.11. Consistent with our objective of a fair comparison with established baselines, we maintain a timestep shift of 0.0 during the sampling process. The full sampling configuration is summarized in Table 12.

Table 12: Sampling and Inference Hyperparameters.

Parameter	Value
Sampling Method	Euler (ODE Solver)
Sampling Steps	250
ODE Tolerance (atol/rtol)	$10^{-6} / 10^{-3}$
CFG Scale (ω)	15.0
CFG Interval Start	0.11
Timestep Shift	0.0
FID Sample Count	50,000

C.2.4. STAGE 3: LATENT-GUIDED REFINER

The Latent-Guided Refiner bridges the gap between latent-domain semantics and pixel-domain high-frequency fidelity. It serves as a module that restores fine-grained textures by using compact 32-dimensional latents as structural guidance. We employ a PatchGAN (Isola et al., 2017) discriminator for the adversarial loss \mathcal{L}_{adv} to encourage the synthesis of realistic high-frequency textures such as sharp edges and fine fur patterns. Core hyperparameters are summarized in Table 13.

D. Additional Experimental Results

In this section, we provide further results and analysis to validate the robustness and generative performance of RePack.

D.1. Performance without Classifier-Free Guidance

We evaluate RePack on ImageNet 256×256 without classifier-free guidance. As shown in Table 14, RePack achieves a gFID of 3.81 after only 64 training epochs, outperforming VA-VAE (5.14) and the original DiT (9.62). This demonstrates that the compact 32-dimensional semantic manifold provides a cleaner and more effective optimization target, enabling rapid convergence even without external guidance. Although methods such as FAE and RAE achieve lower FID with longer training or larger VAEs, RePack’s strong early-stage performance highlights its advantage for efficient training and fast iteration.

Table 13: Essential Hyperparameters for the Latent-Guided Refiner.

Configuration	Value
Learning Rate	1.0×10^{-4}
Batch Size	64
Latent Dimension (z)	32
Input Channels	35
LPIPS weight (λ_{lips})	1.0
GAN weight (λ_{adv})	0.5

Table 14: Class-conditional Image Generation Results **without CFG** for DiT-XL/1 on ImageNet 256×256 .

Method	Epochs	gFID ↓	IS ↑
AR Models			
LlamaGen (Sun et al., 2024)	300	9.38	112.9
MAR (Li et al., 2024b)	800	2.35	227.8
LDMs			
DiT (Peebles & Xie, 2023)	1400	9.62	121.5
SiT (Ma et al., 2024)	1400	8.61	131.7
VA-VAE (Yao et al., 2025)	64	5.14	130.2
VA-VAE (Yao et al., 2025)	800	2.17	205.6
FAE (Gao et al., 2025)	64	2.55	189.9
RAE (DiT-XL) (Zheng et al., 2025)	800	1.87	209.7
RePack	64	3.81	151.4
RePack + Refiner	64	3.79	152.5

D.2. Extended Analysis of Latent Representations

In this section, we provide the mathematical formulation for the spectral decomposition analysis presented in the main text (Section 4.4) and offer a more detailed discussion on the structural properties of the learned latent spaces.

D.2.1. SPECTRAL DECOMPOSITION

To analyze the frequency characteristics, we decompose the latent map z into low- and high-frequency components via spectral filtering. We define a binary low-pass mask M_r based on a normalized cutoff $r \in [0, 1]$:

$$M_r(u, v) = \mathbf{1} \left[\sqrt{(u - u_0)^2 + (v - v_0)^2} \leq r \cdot \min(h, w)/2 \right], \quad (9)$$

where (u_0, v_0) is the spectral center. The decomposition is then computed via the 2D FFT (\mathcal{F}) and its inverse (\mathcal{F}^{-1}):

$$z_{\text{low}} = \mathcal{F}^{-1}(\mathcal{F}(z) \odot M_r), \quad z_{\text{high}} = \mathcal{F}^{-1}(\mathcal{F}(z) \odot (1 - M_r)). \quad (10)$$

In our experiments, we set $r = 0.25$ to separate the primary semantic layout from high-frequency details.

Table 15: **Taxonomy of Latent Space Construction Paradigms.** We categorize recent approaches based on their utilization of Vision Foundation Models (VFMs) and training strategies.

Category	Representative Methods	Core Mechanism	Key Advantages	Trade-offs
I. Native Structural	EQ-VAE (Kouzelis et al., 2025), SE (Skorokhodov et al., 2025), DCAE-1.5 (Chen et al., 2025b)	Optimizes latent structure via internal constraints (e.g., equivariance, spectral regularity) without VFM guidance.	Self-contained training; effective disentanglement of structure and detail.	Lacks high-level semantic priors, resulting in slower DiT convergence compared to VFM-assisted methods.
II. VFM-Aligned	VA-VAE (Yao et al., 2025), REPA-E (Leng et al., 2025)	Indirectly leverages VFMs to regularize VAE training via alignment losses.	Produces a structured latent space that balances semantics and reconstruction.	Increases the complexity and computational cost of the VAE training stage.
III. Direct VFM	RAE (Zheng et al., 2025), SVG (Shi et al., 2025b)	Directly utilizes frozen features from pre-trained VFMs (e.g., DINO, CLIP) as latents.	Maximal semantic richness; bypasses expensive encoder training by utilizing frozen VFM features.	High dimensionality leads to feature redundancy; overlooks the encoder’s fundamental role in information compression.
IV. Pixel / PDM	DeCo (Ma et al., 2025), JiT (Li & He, 2025), PixelDiT (Yu et al., 2025b)	Models semantics via patchified inputs and restores high-freq details using specialized components.	End-to-end training; decouples semantics from texture.	Slower convergence speed; requires dedicated high-resolution learning modules.

D.2.2. PRINCIPAL COMPONENT ANALYSIS (PCA)

To visualize the latent structure, we apply PCA to a single latent feature map $z \in \mathbb{R}^{d \times h \times w}$. We flatten z into N feature vectors ($N = h \cdot w$) and project them onto the top-3 principal components to obtain a compressed representation $Y \in \mathbb{R}^{N \times 3}$. These three components are then channel-wise min-max normalized to $[0, 1]$, reshaped to $(h, w, 3)$, and assigned to the R, G, and B channels to form the final visualization.

D.2.3. POSITIONING REPACK: SYNERGY OVER COMPETITION

As illustrated in Table 15, each paradigm offers distinct advantages and trade-offs. For instance, Category II methods like VA-VAE have been successfully validated in large-scale production models (e.g., HunyuanImage-2.1 (Team, 2025)), proving the effectiveness of aligned representations. It is worth noting that the analysis in Section 4.4 is not intended to dismiss other methods, but rather to understand the implications of different design choices from the perspective of representation structure. Building upon these insights, our work explores a complementary direction: **how can we synthesize the strengths of these distinct paradigms?**

The spectral analysis in Section 4.4 (Main Text) reveals our design philosophy. RePack integrates the foundational principles of these paradigms into a unified framework:

- Insight from Cat. II (Compression):** We follow the common view that compressing the latent manifold helps simplify the modeling task. RePack adopts this idea by projecting features into a compact low-dimensional space ($d = 32$).
- Insight from Cat. III (Semantic Fidelity):** We observe that directly utilizing signals from frozen VFMs preserves *higher semantic purity* compared to distilling them into a complex learnable encoder.
- Insight from Cat. IV (Decoupling):** We follow a frequency-decoupled design. High-frequency details are handled by a dedicated Refiner.

RePack’s experimental results demonstrate that synthesizing the compression mechanism of VAEs, the semantic purity of frozen VFMs, and the decoupling strategy of PDMs provides a highly efficient solution for generative modeling.

D.3. Extended Analysis of Representation Redundancy

We provide more detailed mathematical formulation and further analysis of the redundancy analysis presented in Section 2.2.

D.3.1. SPECTRAL ANALYSIS FORMULATION

Let $\mathcal{D} = \{x_1, \dots, x_N\}$ be a subset of images sampled from ImageNet-1K. We extract the raw feature tokens using the frozen VFM encoder \mathcal{E}_ϕ . Let $\mathbf{z}_i \in \mathbb{R}^D$ denote the flattened feature vector for image x_i , where $D = 768$ for ViT-B. We

construct the centered feature matrix $\mathbf{Z} \in \mathbb{R}^{M \times D}$, where M is the total number of tokens across the dataset. The covariance matrix is given by:

$$\mathbf{C} = \frac{1}{M-1} \mathbf{Z}^\top \mathbf{Z}. \quad (11)$$

We perform the eigen-decomposition of \mathbf{C} such that $\mathbf{C}\mathbf{v}_j = \lambda_j \mathbf{v}_j$, where $\lambda_1 \geq \lambda_2 \geq \dots \geq \lambda_D \geq 0$ are the eigenvalues representing the variance along each principal component.

D.3.2. EFFECTIVE DIMENSIONALITY

To quantify the information content, we define the Cumulative Explained Variance (CEV) ratio at dimension k as:

$$R(k) = \frac{\sum_{j=1}^k \lambda_j}{\sum_{j=1}^D \lambda_j}. \quad (12)$$

Our empirical evaluation on DINOv3 features yields the following observations:

- **Significant Sparsity:** At $k = 32$, we observe $R(32) \approx 0.77$. This implies that a subspace utilizing only 4.1% of the feature dimensions captures nearly 80% of the semantic energy.
- **Heavy-Tail Distribution:** The eigenvalue spectrum exhibits a sharp decay followed by a long tail, where λ_j for $j > 32$ corresponds to marginal variance contributions (approx. 23%), largely attributed to high-frequency texture noise.

In contrast, the packed representation (RePack) exhibits a near-linear CEV curve relative to its normalized dimensions. This indicates a more uniform distribution of variance across the projected channels, demonstrating that RePack maximizes information entropy within the compact manifold and effectively eliminates inter-channel redundancy.

D.3.3. ALIGNMENT WITH LINEAR PROJECTION

The validity of using PCA to motivate our design lies in the architecture of RePack itself. The RePack Projector \mathcal{P}_θ is defined as a learnable linear transformation $W \in \mathbb{R}^{D \times d}$. According to the Eckart-Young-Mirsky theorem (Eckart & Young, 1936), the optimal rank- d linear approximation of the matrix \mathbf{Z} (in the Frobenius norm sense) is the truncation of its Singular Value Decomposition (SVD) to the top- d singular values.

Therefore, the PCA result provides the theoretical upper bound for the information capacity of our linear projector. The observed *elbow* around $d = 32$ serves as the optimal operating point that balances semantic retention ($R(32) \approx 0.77$) against the computational efficiency of the subsequent DiT training.

D.4. Linear Probing Evaluation

To assess the semantic discriminability of the learned latent representations, we conduct a linear probing evaluation on the ImageNet-1K benchmark. We freeze the pre-trained encoder and train a supervised linear classifier on top of the extracted features.

D.4.1. EXPERIMENTAL SETUP

Given an input image x , let $Z = \mathcal{E}(x) \in \mathbb{R}^{d \times h \times w}$ denote the frozen feature map. We define the linear probing objective as mapping the spatially averaged features directly to class logits $\mathbf{l} \in \mathbb{R}^C$:

$$\mathbf{l} = \mathbf{W} \left(\frac{1}{hw} \sum_{i=1}^h \sum_{j=1}^w Z_{:,i,j} \right) + \mathbf{b}, \quad (13)$$

where the term in parentheses represents the Global Average Pooling (GAP) operation. $\mathbf{W} \in \mathbb{R}^{C \times d}$ and $\mathbf{b} \in \mathbb{R}^C$ are the learnable weights and bias of the linear classifier ($C = 1000$), optimized via standard cross-entropy loss while keeping \mathcal{E} frozen. The parameters $\{\mathbf{W}, \mathbf{b}\}$ are optimized while keeping \mathcal{E} frozen. The linear classifier is trained for 200 epochs using SGD with a momentum of 0.9 and no weight decay. We employ a Cosine Annealing learning rate schedule, initialized at 0.1 and decaying to 0.0001. All experiments are performed using a batch size of 2048.

D.4.2. RESULTS AND ANALYSIS

Table 16 reports the detailed performance metrics, including Training Accuracy, Validation Accuracy, and the number of trainable parameters in the linear probe.

Table 16: **Linear Probing Performance on ImageNet-1K.** Note that the classifier for DINOv3-B has $24\times$ more parameters compared to the RePack variants.

Method	Input Feature Shape (d)	Linear Layer Params (M)	Compression Ratio	Train Acc. (%)	Val Acc. (%)
DINOv3-B-RePack	1×32	0.03	$24\times$	45.24	42.48
PCA-RePack	1×32	0.03	$24\times$	58.68	56.13
VA-VAE (Yao et al., 2025)	1×32	0.03	$24\times$	31.00	28.43
Standard VAE	1×32	0.03	$24\times$	0.83	0.85
DINOv3-B	1×768	0.77	$1\times$	83.21	82.56

The results highlight three key observations:

- Superiority over Baselines:** RePack achieves a validation accuracy of **42.48%**, outperforming VA-VAE (28.43%) and the Standard VAE (0.85%). This confirms that our projection-based compression effectively retains core semantic structures that are often lost in standard reconstruction-based VAE training.
- Efficiency Trade-off:** While raw DINOv3 features achieve 82.56% accuracy, this comes at the cost of a 768-dimensional space. The linear classifier for DINOv3 requires **0.77M** parameters, whereas RePack’s classifier uses only **0.03M**. Despite a $24\times$ reduction in dimensionality and classifier capacity, RePack maintains reasonable separability.
- Reference to PCA:** PCA-RePack (56.13%) can be regarded as the theoretical upper bound of linear separability within this 32-dimensional subspace, as justified in Appendix D.3.3 based on the Eckart–Young–Mirsky theorem. The performance gap between RePack (42.48%) and PCA arises from an intentional design trade-off. Unlike PCA, which is optimized to maximize variance, RePack compromises some degree of semantic separability in order to satisfy the spatial reconstruction constraints required for image generation. Nevertheless, extensive generative experiments demonstrate that the semantic information preserved by RePack remains stable and is fully sufficient to support high-quality DiT synthesis.

D.4.3. GENERALIZATION OF THE REFINER TO OTHER LATENT SPACES

As shown in Table 17, While the Refiner consistently lowers the reconstruction error (rFID) for all methods, it degrades the generative performance (gFID) for both VA-VAE (2.11 \rightarrow 2.86) and SD-VAE (2.27 \rightarrow 2.51). This contrasts with RePack, where the Refiner yields a significant boost (1.82 \rightarrow 1.65).

Hypothesis: Distribution Mismatch. We hypothesize that the performance drop mainly comes from a mismatch between the Refiner’s training and inference conditions.

The Refiner is trained using clean, ground-truth latents and their decoded images, whereas at inference, it must operate on latents generated by the DiT, which are noisier and follow a different distribution. For SD-VAE and VA-VAE, this gap is especially large: their ground-truth latents are detailed (rFID \approx 0.2–0.6), which likely leads the Refiner to depend on precise cues that are no longer reliable once the latent is generated (gFID $>$ 2.1).

In contrast, RePack builds on VFM features that naturally emphasize high-level semantics rather than low-level textures. The compact bottleneck ($d = 32$) further suppresses fine-grained information, intentionally producing a latent representation

Table 17: **Effectiveness of the Latent-Guided Refiner across different latent spaces.** While the Refiner consistently improves reconstruction (rFID), it degrades generation performance (gFID) for VA-VAE and SD-VAE, unlike RePack.

To investigate the generalization of the Latent-Guided Refiner, we apply it to VA-VAE (Yao et al., 2025) and the standard SD-VAE (Peebles & Xie, 2023).

Method	Backbone	rFID \downarrow	gFID \downarrow
RePack (Ours)	DiT-XL/1 (64 ep)	0.83 \rightarrow 0.69	1.82 \rightarrow 1.65
VA-VAE (Yao et al., 2025)	DiT-XL/1 (64 ep)	0.28 \rightarrow 0.22	2.11 \rightarrow 2.86 \uparrow
SD-VAE (Peebles & Xie, 2023)	DiT-XL/2	0.60 \rightarrow 0.40	2.27 \rightarrow 2.51 \uparrow

that retains semantic structure while discarding detailed appearance. This representation matches the role of the Refiner, which is responsible for reconstructing high-frequency details from coarse semantic cues. As a result, unlike other VAEs where semantics and texture are entangled, RePack enforces a clear separation of responsibilities, allowing the Refiner to function as a necessary and well-aligned component. Nevertheless, designing a universal Refiner is a promising direction for future work, which we plan to further explore.

D.5. Efficiency under Resource Constraints.

It is worth noting that our current experiments are constrained by limited computational resources, restricting our training to a maximum of 80 epochs. In contrast, most state-of-the-art baselines (e.g., RAE (Zheng et al., 2025), SiT (Ma et al., 2024), MAR (Li et al., 2024b)) rely on prolonged training schedules ranging from 800 to 1,600 epochs to fully converge. Despite this significant disparity (training for only ~5-10% of the standard schedule), RePack equipped with the Refiner achieves a highly competitive FID of 1.61. As shown in Table 1, this performance is comparable to several competitive methods trained for hundreds of epochs. We acknowledge this as a current limitation and plan to extend the training in future work.

Furthermore, these constraints on compute and time also limited our scope regarding Text-to-Image (T2I) generation. We acknowledge this limitation. Extending RePack to large-scale T2I generation remains a primary direction for our future research.

E. Extended Discussion on Concurrent Approaches

In this section, we provide a comparison with concurrent works that similarly leverage Vision Foundation Models (VFMs) for generation.

Integrating Vision Foundation Models (VFMs) into generative pipelines has recently attracted increasing attention. Concurrent with our work, several studies (Bi et al., 2025; Zhang et al., 2025a; Gao et al., 2025) independently explore similar directions. The emergence of these efforts reflects a shared view in the community that the semantic representations learned by VFMs can play an important role in improving the efficiency of generative models.

While sharing this broader motivation, these concurrent works diverge in their specific methodologies and trade-offs.

VFM-VAE (Bi et al., 2025) focuses on architectural modifications to the decoder to handle coarse features. While effective, it requires more training to align the representation, achieving an FID of 1.62 after 640 epochs. In comparison, RePack achieves a comparable FID of 1.61 (with Refiner) in 80 epochs.

FAE (Gao et al., 2025) introduces attention-based adapters to bridge the feature gap, leveraging massive backbones like DINOv2-Giant to ensure performance. RePack achieves competitive results (FID 1.82 vs. 1.87 at 64 epochs) using a standard ViT-B backbone and a lightweight linear projector, offering a more parameter-efficient solution.

PS-VAE (Zhang et al., 2025a) adopts a joint fine-tuning strategy and compresses features to 96 channels. Although direct generation comparison is unavailable due to differing benchmarks, our empirical analysis suggests that a compact 32-channel manifold (vs. 96) is more beneficial to rapid DiT convergence. Furthermore, it remains unclear whether fine-tuning the VFM consistently preserves the generality of VFM representations, as it may lead to dataset-specific adaptation.

Ultimately, we acknowledge that each of these concurrent approaches offers unique insights and advantages to the field. We hope that RePack, alongside these pioneering works, contributes to a broader research direction that pushes the boundaries of efficient, VFM-driven generative models.

F. Further Clarifications

In this section, we provide clarifications on the conceptual visualization, feature dimensionality, reconstruction versus generation quality, and reproducibility of RePack.

F.1. Clarification on Conceptual Visualization

We clarify that the schematic illustration of the optimization landscape (Figure 2, bottom) is AI-generated and is intended solely to convey our design philosophy. The actual feature spaces operate in much higher dimensions. The raw VFM space (DINOv3-B) contains 768 channels, and the compressed RePack manifold still consists of 32 channels. Direct visualization

of such high-dimensional spaces is difficult. Therefore, we adopt a dimensional analogy, the rugged 3D terrain represents the complexity of the high-dimensional space, and the glowing planar slice simulates the projection onto a lower-dimensional manifold. Ultimately, this illustration is meant to convey that, compared to the more simpler optimization path in the compact RePack space, fitting a distribution in the large and redundant raw VFM space requires a larger and complex search space.

F.2. Clarification on Feature Dimensionality and Redundancy

In the Introduction Section (Main Text), we note that standard VFM features (e.g., DINOv3 with shape $768 \times H/16 \times W/16$) contain the same number of numerical elements as the original RGB image ($3 \times H \times W$). This comparison is intended to highlight the **dimensional redundancy** of the raw VFM latent space, rather than to equate the information content of VFM features with raw pixels. While VFM features are semantically structured and low-rank, standard VFM encoders embed them into a high-dimensional space (e.g., 768 channels), resulting in a clear dimensional redundancy.

F.3. Clarification on Reconstruction vs. Generation Quality

We frankly acknowledge that, compared to VAEs trained end-to-end in pixel space, using frozen VFM features leads to weaker reconstruction fidelity. However, prior work such as SVG (Shi et al., 2025b) shows that pursuing better reconstruction (e.g., reducing rFID from 1.17 to 0.65) may yield only marginal improvements in generation quality (gFID 6.12 \rightarrow 6.11; Table 4 in the SVG paper).

RePack emphasizes semantic packing at the encoding stage, while assigning high-frequency detail recovery to the Refiner. This design is motivated by our goal of enabling efficient generative modeling while maintaining high image fidelity. As a result, this decoupled strategy improves both reconstruction performance (rFID from 0.83 to 0.69) and generation quality (gFID from 1.82 to 1.65).

Nevertheless, we also acknowledge that this strategy may introduce limitations when applied to downstream tasks such as image editing. In future work, we plan to explore more flexible spatial control mechanisms within this framework to maintain generation efficiency while extending its applicability to fine-grained editing and other downstream tasks.

F.4. Reproducibility and Code Availability

We emphasize the importance of reproducibility and open-source community engagement. To ensure that the community can fully reproduce our results, we are committed to releasing our complete implementation. This includes the source code, training configurations, and pretrained model checkpoints, which will be made publicly available after being properly organized upon the paper’s acceptance.

G. Additional Visualizations

G.1. Extended Generated Samples

Figure 8 presents samples generated by RePack-DiT-XL/1 with the Latent-Guided Refiner after 64 training epochs.

G.2. Training Progression

Figure 9 visualizes the generation quality of RePack-DiT-XL/1 across different training stages, covering from 8 to 64 epochs. Notably, the model establishes a coherent semantic structure as early as epoch 8, producing recognizable object shapes and layouts.

G.3. Extended Analysis of Latent Representations

Figure 10 provides extended PCA visualizations and spectral decompositions, further verifying that RePack produces more semantically coherent and structurally clean latent representations.

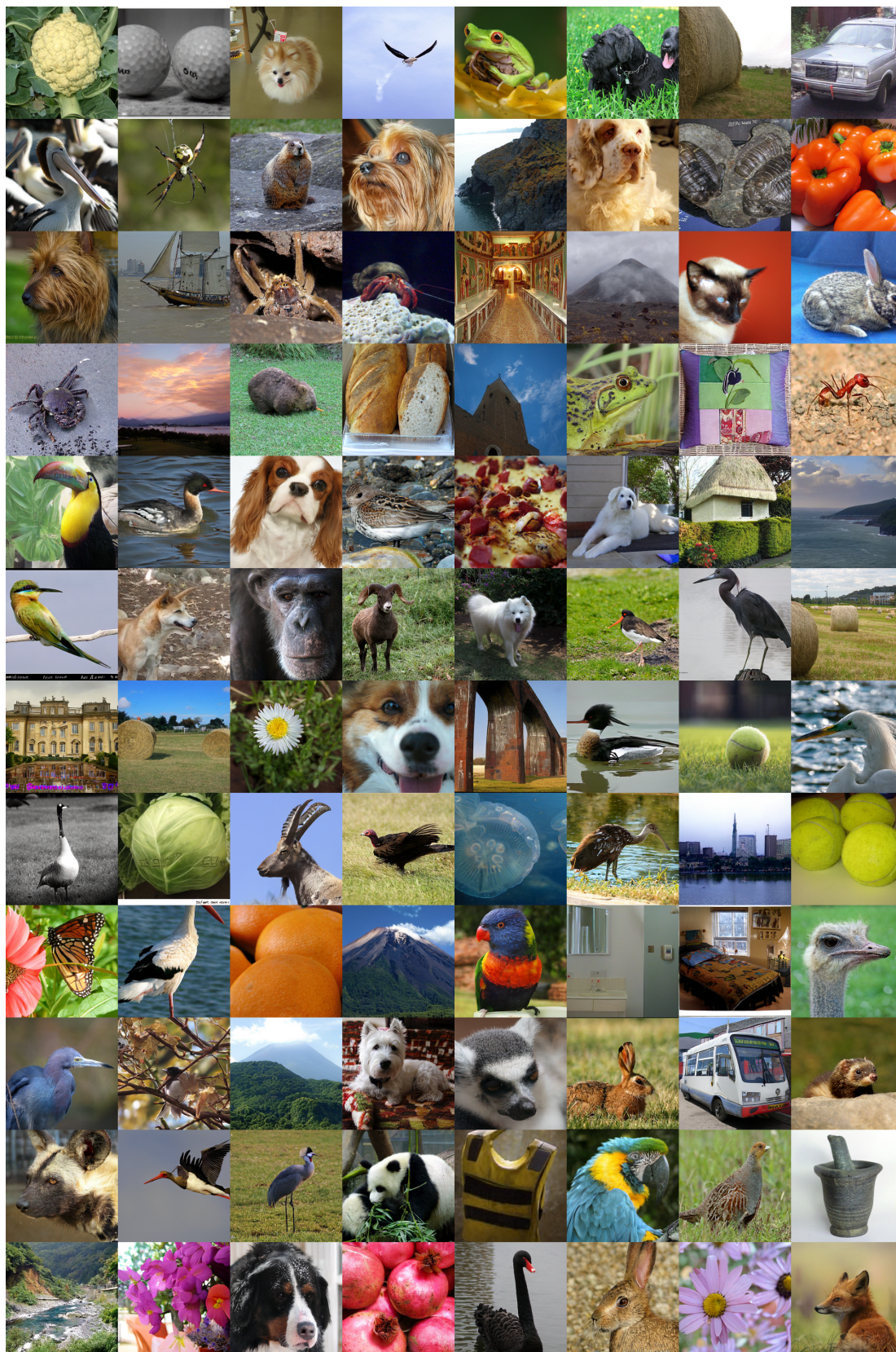


Figure 8: **Extended Generated Samples (64 Epochs)**. Samples generated by RePack-DiT-XL/1 + Refiner on ImageNet 256×256 .

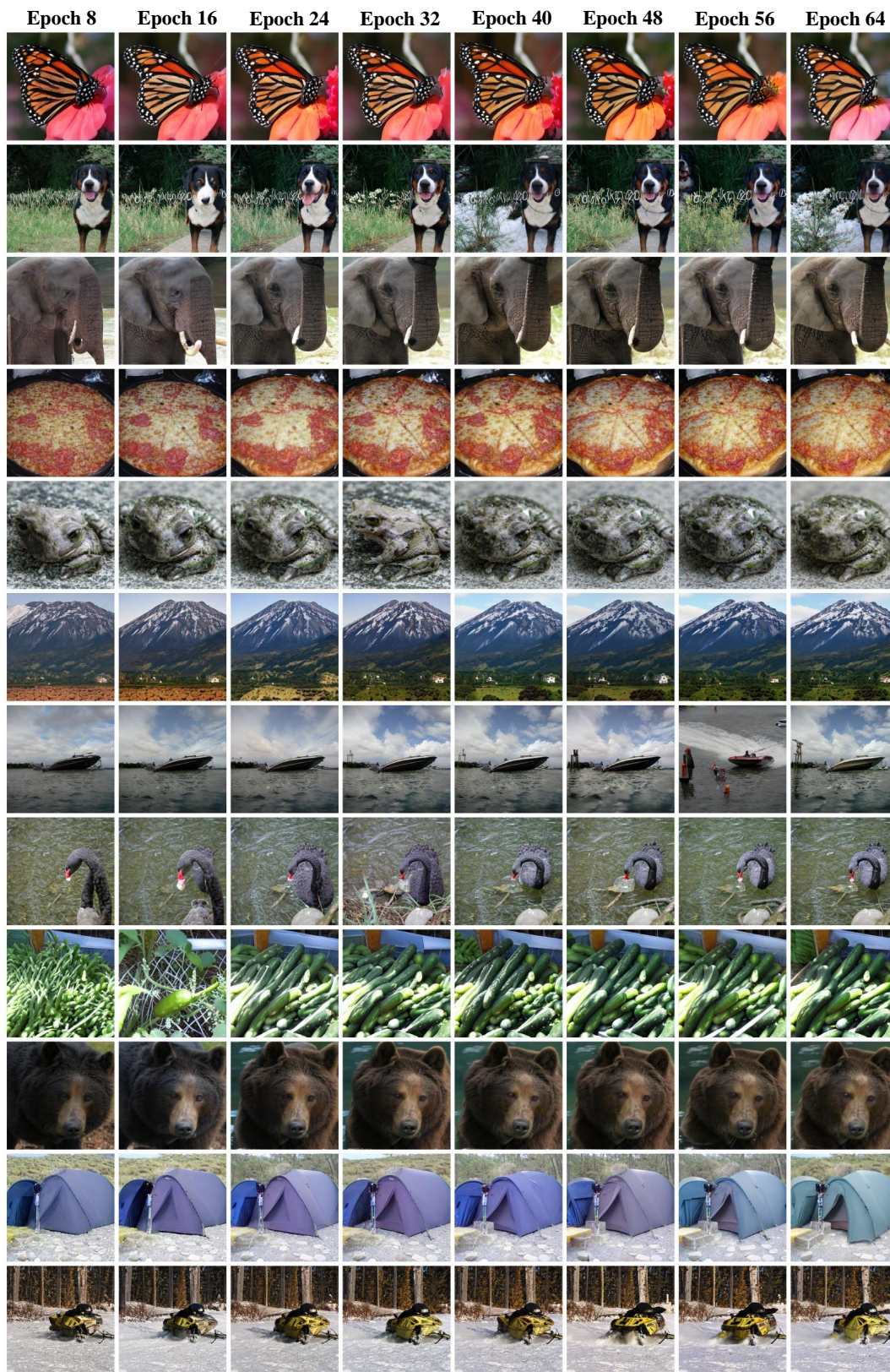


Figure 9: **Visualization of Training Progression.** Samples generated by RePack-DiT-XL/1 at 8, 16, 24, 32, 40, 48, 56 and 64 epochs. The model exhibits rapid convergence, forming stable semantic structures at a very early stage.



Figure 10: **Extended Visual Analysis of Latent Representations.** Complementing Figure 7 in the main text, this figure provides additional visualizations. **Left:** Input images. **Middle:** PCA visualizations of latents from a Standard VAE (trained w/o VFM guidance), VA-VAE, and RePack. **Right:** Spectral decomposition of VA-VAE and RePack latents.